# Simultaneous electrokinetic flow and dielectrophoretic trapping using perpendicular static and dynamic electric fields

**ARTICLE** *in* MICROFLUIDICS AND NANOFLUIDICS · NOVEMBER 2013

Impact Factor: 2.53 · DOI: 10.1007/s10404-013-1175-z



**4 AUTHORS**, INCLUDING:

Michael B Sano
Stanford University
**37** PUBLICATIONS **460** CITATIONS
SEE PROFILE

Blanca Lapizco-Encinas
Rochester Institute of Technology
**94** PUBLICATIONS **1,281** CITATIONS
SEE PROFILE

Rafael V Davalos
Virginia Polytechnic Institute and State Uni…
**108** PUBLICATIONS **1,971** CITATIONS
SEE PROFILE

Microfluid Nanofluid (2013) 15:599–609
DOI 10.1007/s10404-013-1175-z

RESEARCH PAPER

# Simultaneous electrokinetic flow and dielectrophoretic trapping using perpendicular static and dynamic electric fields

**Michael B. Sano · Roberto C. Gallo-Villanueva · Blanca H. Lapizco-Encinas · Rafael V. Davalos**

Received: 1 July 2012 / Accepted: 21 November 2012 / Published online: 29 March 2013


**Abstract** Microfluidics is a rapidly growing field that offers great potential for many biological and analytical applications. There are important advantages that miniaturization has to offer, such as portability, shorter response times, higher resolution and sensitivity. There is growing interest on the development of microscale techniques. Among these, electrokinetic phenomena have gained significant importance due to their flexibility for handling bioparticles. Dielectrophoresis (DEP), the manipulation of particles in non-uniform electric fields due to polarization effects, has become one of leading electrokinetic techniques. DEP has been successfully employed to manipulate proteins, DNA and a wide array of cells, form bacteria to cancer. Contactless DEP (cDEP) is a novel dielectrophoretic mode with attractive characteristics. In cDEP, non-uniform electric fields are created using insulating structures and external electrodes that are separated from the sample by a thin insulating barrier. This prevents bioparticle damage and makes cDEP a technique of choice for many biomedical applications. In this study, a combination of cDEP generated with AC potentials and electrokinetic liquid pumping generated with DC potentials is employed to achieve highly controlled particle trapping and manipulation. This allows for lower applied potentials than those used in traditional insulator-based DEP and requires a simpler sytem that does not employ an external pump. This is the first demonstration of electrokinetic (EK) pumping in which the driving electrodes are not in direct contact with the sample fluid. Multiphysics simulations were used to aid with the design of the system and predict the regions of particle trapping. Results show the advantages of combining AC-cDEP with DC EK liquid pumping for dynamic microparticle trapping, release and enrichment.

**Keywords** Microfluidics · Numerical model · Electrokinetic micropump · Electro-osmosis · Contactless dielectrophoresis

M. B. Sano (✉) · R. C. Gallo-Villanueva · R. V. Davalos
School of Biomedical Engineering and Sciences,
Virginia Tech-Wake Forest University, 330 ICTAS Building,
Stanger Street (MC 0298), Blacksburg, VA 24061, USA
e-mail: sano@vt.edu

R. C. Gallo-Villanueva
BioMEMS Research Chair, Tecnólogico de Monterrey,
64849 Monterrey, NL, Mexico

B. H. Lapizco-Encinas
Department of Chemical and Biomedical Engineering,
Rochester Institute of Technology, Rochester,
NY 14623-5604, USA

## 1 Introduction

Microfluidics is rapidly becoming the tool of choice for many complex biological applications. The small length scale allows for high control over convection and diffusion transport, reduced volumes decrease the quantity of sample and reagents consumed, and higher resolution and sensitivity are obtained. The low Reynolds number due to device dimensions ensures laminar flow in all, but the most extreme circumstances. This produces predictable flow patterns that are ideal for separations and analysis, since low to negligible mixing is induced (Whitesides 2006).

Electrokinetic (EK) techniques are one of the main pillars of microfluidics as analytical systems. These techniques have great potential for handling bioparticles, from macromolecules to cells. Isotacophoresis and isoelectric focusing have found important applications in protein separations (Ugaz and Christensen 2007). One important

characteristic of microanalytical EK methods is that intact microorganisms can be analyzed. For example electrotaxis, the movement of adherent cells in response to an electric field, has been used to guide the migration of neural stem cells (Feng et al. 2012) and lung cancer cells in 3D scaffolds (Sun et al. 2012). Electrorotation is another important electrokinetic method employed successfully for cell assessment that allows extracting dielectric properties (Voyer et al. 2010). Electrical impedance has also been employed in microdevices for the detection and quantification of bacterial cells in suspensions, with great application in food safety analysis (Yang and Bashir 2008). A number of excellent reviews which describe the assessment and manipulation of cells with electric fields in depth have been published recently (Bao et al. 2008; Gagnon 2011; Voldman 2006).

Among the family of EK techniques, dielectrophoresis (DEP), the motion of a particle due to polarization effects in the presence of a non-uniform electric field, has proven to have an enormous potential for applications with cells (Gagnon 2011). Microfluidic applications exploiting DEP originally used electrodes patterned on the bottom of a channel which trapped cells as they were driven past by pressure flow (Docoslis et al. 1997). Though design and fabrication of microdevices which apply to this technique may be complex and expensive, its applications have been demonstrated as effective means to trap DNA (Regtmeier et al. 2010), viruses (Ermolina et al. 2006), and bacterial (Hughes and Hoettges 2008) and mammalian cells (Yang et al. 2010) as well as for identification of antigen expression and blood typing (Leonard and Minerick 2011). Three-dimensional carbon electrodes, which require a less extensive fabrication process, have been used as an alternative to metal electrodes. Carbon-electrode dielectrophoresis (carbon-DEP) has been used to trap cells such as yeast and bacteria with the significant advantage of providing higher throughputs due to the 3D configuration and allowing for centrifugal pumping in a CD-like platform (Jaramillo et al. 2010; Martinez-Duarte et al. 2010, 2011). However, electrode-based DEP can have some drawbacks such as loss of functionality due to fouling, which is common when working with bioparticles, such as cells. Additionally, direct contact between the electrodes and the sample can lead to cell damage (Moncada-Hernández and Lapizco-Encinas 2010; Shafiee et al. 2009).

As an alternative, a non-uniform electric field can also be produced by placing insulating structures within a channel and using two external electrodes placed at the inlet and outlet of a channel (Cummings and Singh 2003). In this configuration, DC fields are typically used and the electric field drives electro-osmotic flow, while the insulating structures distort the electric field distribution inducing a DEP force on any particle within the fluid. This technique, known as the insulator-based dielectrophoresis (iDEP) is advantageous as the dielectrophoretic force produced extends to the entire height of the channel allowing for 3D particle manipulation (Baylon-Cardiel et al. 2009). Recently, there has been an important progression of iDEP studies, demonstrating its application as an effective method to trap single cells (Bhattacharya et al. 2011), concentrate proteins (Ivory and Srivastava 2011) and DNA (Gallo-Villanueva et al. 2009), separate and concentrate mixtures of particles (Gallo-Villanueva et al. 2011; Moncada-Hernández and Lapizco-Encinas 2010), interrogate cell viability (Gallo-Villanueva et al. 2011), and blood types (Srivastava et al. 2011). These systems have also been used with low frequency AC potential, where the shape of the applied signal is an additional parameter to control particle manipulation (Baylon-Cardiel et al. 2010). Important progress on the mathematical modeling of iDEP systems has also been reported allowing for the prediction of particle selectivity, trapping and concentration within a microchannel (Baylon-Cardiel et al. 2009; Chávez-Santoscoy et al. 2011). The majority of iDEP studies have employed fairly high DC potentials to manipulate particles, from proteins (Lapizco-Encinas et al. 2008) to cells (Moncada-Hernández et al. 2011). The resulting Joule heating and electrothermal flow effects (Hawkins and Kirby 2010; Sridharan et al. 2011) are important challenges in iDEP that lead to electrochemical effects and bubble generation. These high DC potentials can also result in significant pH changes that can lead to bioparticle denaturation or cell death (Gencoglu et al. 2011).

Despite these challenges, iDEP offers great potential and flexibility for successful cell manipulation. Due to that, other recent techniques related to iDEP have been developed. Insulator gradient dielectrophoresis (g-iDEP) employs tapered microchannels with insulating saw-tooth structures along the wall, this method has been successfully employed for separating bacteria and assessing blood cells (Jones et al. 2011; Pysher and Hayes 2007). Contactless DEP (cDEP) is another successful technique where insulating structures distort the distribution of an electric field to generate DEP forces; however, this method has a significant advantage, since the sample does not come in direct contact with the electrodes.

In cDEP, AC electric potentials are applied employing electrodes immersed in a highly conductive solution, which is isolated from the sample channel by thin insulating membranes. The capacitive nature of these membranes allows for the transmission of AC signals into a main sample channel. Electric fields are generated across the microchannel width, perpendicular to the particle flow, allowing for highly selective particle manipulation, since positive and negative DEP can be employed (Sano et al. 2011). Contactless DEP has found a special niche in

biomedical and clinical applications. Recently, cDEP has been used to isolate live cancer cells from beads of similar size (Shafiee et al. 2010a), dead cells of the same cell line (Shafiee et al. 2010b), live cells from dissimilar cell lines (Henslee et al. 2011), and dilute blood samples (Sano et al. 2011).

A significant challenge with current cDEP devices is the requirement of a syringe pump to accurately drive pressure driven flow of samples. This increases the peripheral equipment count and impacts the portability of the devices. In conjunction with the development of lab-on-a-chip technologies, there has been a surge in microscale pumping techniques aimed at eliminating the need for external pumps. These devices can be generalized into two main groups; mechanical displacement, and electro-magneto-kinetic pumps (Iverson and Garimella 2008). Mechanical displacement pumps apply a pressure force on a flexible diaphragm (Machauf et al. 2005) or into peristaltic (Lin et al. 2007) and rotary pumping geometries (Matteucci et al. 2006). In contrast, electro-magneto-kinetic pumps directly transfer electromagnetic energy into the fluid to achieve a steady-state flow. Electro-hydrodynamic devices induce a fluid body force through the interaction of a dielectric fluid's space charge density and a non-uniform electric field (Iverson and Garimella 2008). These usually require a gradient in the conductivity or permittivity within the fluid, caused by unmixed fluid layers, suspended particles, or because of anisotropic heating (Felten et al. 2006). Magnetohydrodynamic pumps use perpendicular electric and magnetic fields to induce a Lorentz force in the fluid that acts to drive the fluid in a direction perpendicular to both applied fields (Homsy et al. 2007). Alternatively, electro-osmotic pumping techniques rely on the surface charge that forms when fluids come into contact with a channel wall (Tandon et al. 2008). This simple technique only requires the formation of an electric field along the direction of desired fluid motion.

The present work shows the combination of cDEP and EK pumping for highly controlled microparticle manipulation in a microchannel with a set of six electrodes (Fig. 1). AC potentials applied across the width of a microchannel were used to achieve dielectrophoretic trapping at the center of the main channel in an array of cylindrical insulating structures. EK pumping was created by generating a DC potential drop across side channels separated from the sample channel by thin membranes in a contactless manner. This established a DC potential drop across the length of the sample microchannel to achieve EK pumping. Driving the fluid electrokinetically was chosen due to its simple structure, ease of fabrication, fast response time, and the ease of integration with other microcomponents and software controls. Application of an AC potential perpendicular to the electrokinetic flow, allowed for dynamic particle trapping and releasing by reduction or removal of the applied potential. This configuration eliminates the need of a micropump, simplifying the system and enhancing portability (Srivastava et al. 2011). The performance of the system was simulated employing COMSOL Multiphysics to aid on the design of the microdevice. The results, from both experiments and simulations, demonstrate the important advantages for selective and highly controlled trapping, enriching and manipulation of microparticles at much lower applied potentials by employing the combination of AC–cDEP with EK pumping.

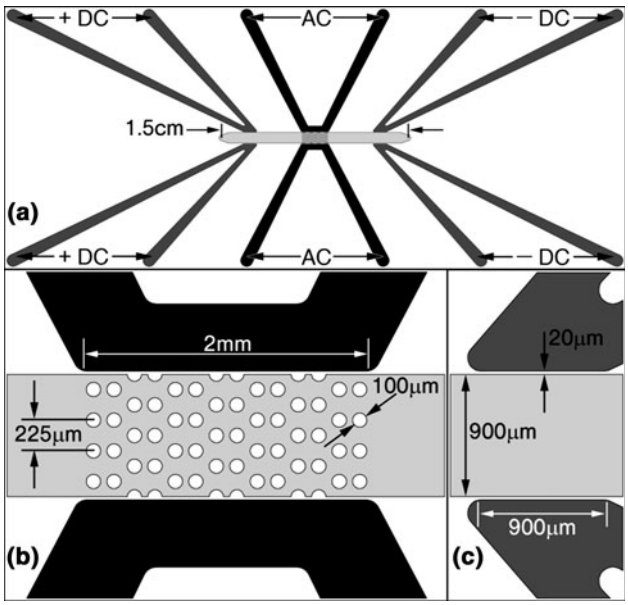


**Fig. 1** Schematic representation of the device used in this study. **a** The device consists of a single sample channel 15-mm long (*light gray*) and six fluid electrode channels. The DC fluid electrode channels (*dark gray*) were used to establish a DC field within the sample channel and generate EO fluid flow. The AC fluid electrode channels (*black*) were used to establish a strong DEP force around (**b**) cylindrical insulating structures within the sample channel, the posts are 100 μm in diameter and the length of the post region is 2.05 mm (**b**–**c**). The barriers which isolate the fluid electrodes from the main sample channel are 20-μm thick

## 2 Theory

### 2.1 Electrokinetics

The application of a uniform electric field to an ionic liquid in a microfluidic field gives rise to electrical double layer (EDL) formation along the channel wall. The ions closest to the channel walls are subject to strong electrostatic forces that cannot be overcome by thermal diffusion. As a result, these ions are statically bound to the surface of the channel forming a fixed Stern layer. The electrostatic force

within the EDL deteriorates further from the channel surface and mobile ions begin to move parallel to the EDL. The net effect of ionic drag caused by the mobile ions on the bulk fluid induces a phenomenon known as electro-osmotic (EO) flow (Barz and Ehrhard 2005). The velocity of an ionic fluid under EO flow ($\mathbf{V}_{eo}$) is estimated by (Barz and Ehrhard 2005)

$$\mathbf{V}_{eo} = \mu_{eo}\mathbf{E} \tag{1}$$

where $\mu_{eo}$ is the electro-osmotic mobility of the ionic fluid and $\mathbf{E}$ is the magnitude of the local electric field. The electro-osmotic mobility

$$\mu_{eo} = \frac{-\varepsilon_m \zeta}{\eta} \tag{2}$$

is a function of the surface potential between the solid and liquid phase ($\zeta$), the viscosity ($\eta$), and permittivity ($\varepsilon_m$) of the fluid (Tandon et al. 2008).

An EDL will additionally form around a charged particle placed in an infinite ionic liquid under a uniform field. The particle will then be driven towards the region of highest potential by a Coulombic force ($\mathbf{F}_c$) which is proportional to the net charge of the particle ($q$) and equal to

$$\mathbf{F}_c = q\mathbf{E} \tag{3}$$

(Kang and Li 2009). This force is known as electrophoresis and the resulting electrophoretic velocity ($\mathbf{V}_{ep}$) of a spherical particle can be calculated using the Huckel equation (Tandon et al. 2008)

$$\mathbf{V}_{ep} = \mu_{ep}E \tag{4}$$

this velocity is a function of the electrophoretic mobility ($\mu_{ep}$) of the cell and the local electric field. The electrophoretic mobility for a spherical particle is defined by the Smoluchowski equation (Baylon-Cardiel et al. 2009)

$$\mu_{ep} = -\frac{\varepsilon_m \zeta_p}{\eta} \tag{5}$$

$\mu_{ep}$ is a function of the surface potential between the particle and the surrounding medium ($\zeta_p$), the permittivity ($\varepsilon_m$), and viscosity ($\eta$) of the surrounding media. The net velocity of the cell as result of these two forces is referred to as the electrokinetic (EK) velocity ($\mathbf{V}_{ek}$) (Baylon-Cardiel et al. 2009; Kwon et al. 2008).

$$\mathbf{V}_{ek} = (\mu_{eo} + \mu_{ep})\mathbf{E} \tag{6}$$

A charged or neutral particle placed in an infinite ionic liquid under a non-uniform field will become polarized and develops a charge distribution across the volume of the particle. The cell will then be driven towards or away from the regions of maximal field gradient by a translational dielectrophoretic force ($\mathbf{F}_{DEP}$) (Pohl 1958)

$$\mathbf{F}_{DEP} = 2\pi\varepsilon_m r_p^3 \mathrm{Re}[K(\omega)]\nabla(\mathbf{E}_{RMS}\cdot\mathbf{E}_{RMS}) \tag{7}$$

where $r_p$ is the radius of the cell, $Re[K(\omega)]$ is the real part of the Clausius–Mossotti (CM) factor, and $\mathbf{E}_{RMS}$ is the amplitude of the electric field. The direction of the translational displacement is dependent on the sign of the CM factor, which is theoretically bound between −0.5 and 1.0 for spherical particles.

A hydrodynamic force, $\mathbf{F}_{DRAG}$, is exerted on the particles as they translate through the fluid.

$$\mathbf{F}_{DRAG} = 6\pi\eta r_p \mathbf{V} \tag{8}$$

where $\mathbf{V}$ is the velocity of the particle relative to the suspending medium. The steady-state velocity of the particles is determined by a balance between the dielectrophoretic forces and Stoke's drag in summation with the EK velocity. In this preliminary study, the effect of acceleration is considered negligible, and the relationship for particle translation is given by:

$$\mathbf{U} = \mathbf{V}_{ek} + \frac{\varepsilon_m r_p^2 \mathrm{Re}[\mathrm{K}(\omega)]}{3\eta}\nabla(\mathbf{E}_{RMS}\cdot\mathbf{E}_{RMS}) \tag{9}$$

## 3 Methods

### 3.1 Sample preparation

Yellow-green fluorescent carboxylate-modified polystyrene microspheres with 1 μm in diameter (Invitrogen, Carlsbad, CA, USA), ex/em 505/515, were resuspended in distilled water to a concentration of $1 \times 10^7$ beads/mL. Final sample fluid had a conductivity of 0.001 S/cm, and a pH of 5.7.

### 3.2 Device fabrication

A silicon master stamp was fabricated on a <100> silicon substrate using photolithography. Deep reactive ion etching (DRIE) was used to etch the silicon master stamp to a depth of 15 μm. Surface roughness was reduced by etching the wafer in tetramethylammonium hydroxide (TMAH) for 5 min. Finally, a thin layer of Teflon was deposited to facilitate stamp removal using typical DRIE passivation parameters. Liquid phase polydimethylsiloxane (PDMS) in a 10:1 ratio of monomers to curing agent (Sylgrad 184, Dow Corning, USA) was degassed under vacuum prior to being poured onto the silicon master and cured for 15 min at 150 °C. Fluidic connections to the channels were punched into the PDMS using 1.5-mm core borers (Harris Uni-Core, Ted Pella Inc., Redding, CA). Glass microscope slides were cleaned with soap and water, rinsed with distilled water, ethanol, and then dried with compressed air.

The PDMS replica was bonded to a clean glass slide after treating with air plasma for 2 min (Model PDC-001, Harrick Plasma, Ithaca, NY, USA).

### 3.3 Device geometry

The device, shown in Fig. 1, consists of a straight sample channel (light gray) and six fluid electrode channels. The sample channel is 15-mm long, 900-μm wide, 20-μm deep, and contains 14 columns of cylindrical pillars, each 100 μm in diameter; the total length of the post region is 2.05 mm. Groups of two columns are offset from the neighboring sets by 225-μm center-to-center in the y-direction and all columns are arranged 150 μm from center-to-center in the x-direction. This geometry was chosen to minimize the effects of DC DEP in the x-direction and maximize the effect of AC DEP.

The fluid electrode channels are divided into two groups. Four DC fluid electrodes (dark gray) are located near the inlet and outlet of the sample channel. These are designed to establish a static DC voltage drop across the sample channel and induce EO flow. The two remaining fluid electrode channels (black) straddle the sample channel near the pillars. These are designed to establish an AC field and induce DEP trapping of particles at the pillars. The barriers separating the sample channel from the six fluid electrodes are 20-μm thick.

### 3.4 Mathematical model and simulations

Two-dimensional geometries were created using AutoCAD (AutoCAD Mechanical 2010, Autodesk Inc, San Rafael, CA, USA). The geometries were imported into COMSOL Multiphysics (Version 4.2, COMSOL Inc., Burlington, MA, USA) where subsets of the AC/DC module were used to solve for the potential distribution, $\phi$, using the governing equation $\nabla\cdot(\sigma^* \nabla\phi) = 0$ where $\sigma^*$ is the complex conductivity, that is defined in terms of the real conductivity and permittivity as: $\sigma^* = \sigma + i\omega\varepsilon$, where $i = \sqrt{-1}$. This model computes the steady-state solution based on a root mean square approximation taking into account the complex permittivity of the materials when relevant. In the electrostatics physics, the boundary conditions were prescribed with uniform potentials of +250 and −250 V for the positive DC and negative DC fluid electrodes, respectively. In the electric currents physics, the boundary conditions were +125 and −125 V on the top and bottom AC fluid electrodes, respectively. This was done to evaluate the time-averaged 0 V potential at the center of the sample channel as anticipated experimentally when a sinusoidal 250 $V_{RMS}$ is applied. The resultant voltages were then summed and used to evaluate the electric field distribution within the sample channel.

All fluid electrodes were defined as phosphate buffered saline (PBS), the sample channel as DI water, and all remaining domains as PDMS. The values for the electrical conductivity and permittivity of the PDMS, DI water, and PBS that were used in this numerical modeling were similar to those reported earlier (Shafiee et al. 2009, 2010a). The DI water and PBS had a relative permittivity of 80 as assumed based on water content. The conductivity of the sample media and PBS were defined as 0.001 and 1.4 S/m, respectively. The relative permittivity and conductivity of the PDMS were defined as 2.7 and $8.33 \times 10^{-13}$ S/m, respectively. The zeta-potential ($\zeta$) between PDMS and the sample was approximated as 1, the viscosity ($\eta$) and permittivity ($\varepsilon_m$) of the sample were set to $8.9 \times 10^{-4}$ N s/m$^2$ and 80 based on their water composition.

The model was solved on a PC with a quad core 3.0 GHz processor and 8 GB of RAM. The mesh was successively refined until the change in the voltage distribution between refinements was less than 1 %. The final mesh used the COMSOL default 'Extremely Fine' with two additional refinements. It contained 2,343,216 elements and required 2 h and 36 min to solve for each parameter set.

### 3.5 Experimental parameters

The devices were placed into a vacuum jar for at least 30 min prior to experiments. The fluid electrode channels were filled with PBS, and then copper wire electrodes were placed in each side channel inlet. The sample channel was primed and 200-μL pipette tips filled with extra sample fluid were used to balance the pressure at the inlet and outlet.

An inverted light microscope (Leica DMI 6000B, Leica Microsystems, Bannockburn, IL) was used to monitor the experiments. A high voltage, low current DC power supply (HVS448 6000D, Labsmith Inc., Livermore, CA) was used to apply +250 and −250 V to the positive and negative DC fluid electrode channels, respectively. An independent channel was used for each polarity and the ground connections from the two channels were connected together. A 250 $V_{RMS}$ 500 kHz signal was then applied across the AC fluid electrode channels. This high voltage, high frequency waveform was produced through a combination of waveform generation, amplification, and step-up transformation. The output signal of a function generator (GFG-3015, GW Instek, Taipei, Taiwan) was passed through a wideband amplification system (AL-50HF-A, Amp-Line Corp., Oakland Gardens, NY, USA). A step-up transformer was then used to achieve output voltages up to 300 $V_{RMS}$. Voltage and frequency were measured using an oscilloscope (TDS-1002B, Tektronics Inc. Beaverton, OR, USA) connected to the output stage of the transformer. 500 kHz

was chosen as the experimental data point as it is at the high end of the capabilities of the high frequency amplification system and coincides within a region of the frequency spectrum where simulations predict the maximum DEP response (results not shown).

Particle enrichment was quantified using image analysis on data acquired before and after the AC signal was applied. The Measure RGB plugin in ImageJ (version 1.43u, National Institutes of Health, USA) was used to quantify the red, green, and blue intensity within the sample channel. These values were averaged and normalized to the area analyzed.

## 4 Results and discussion

### 4.1 Simulation results

Figure 2a shows the time-averaged simulation results obtained by applying a static potential of 500 $V_{DC}$ which was established across the DC fluid electrodes on the extreme ends of the sample channel. The voltage drop across the PDMS is nearly linear across the device (voltage profile at the center of the sample channel is shown in Fig. 3a). As observed in Fig. 3a, the voltage is nearly constant for the first 2.5 mm from the extreme edges of the sample channel. These segments are from the edges of the sample channel to the inner most edges of the DC fluid electrode channels. In the sample channel between the positive and negative DC fluid electrodes, the voltage drops linearly from approximately +95 to −95 $V_{DC}$. A linear fit of this curve predicts that an electric field of 198.7 V/cm is established in the sample channel when 500 $V_{DC}$ is applied across the fluid electrodes. As anticipated due to the symmetry of the device, the potential at the center of the sample channel is 0 $V_{DC}$.

Figure 2b shows the time-averaged electric potential in the device when only an AC voltage of 250 $V_{RMS}$ at 500 kHz is applied to the AC fluid electrodes. There are regions of elevated (or lowered) potential in proximity to the energized fluid electrodes. The magnitude of the voltage drop at the center of the sample channel, from top to bottom, is approximately 20 $V_{RMS}$. The remainder of the device, including a large section of the sample channel, has no substantial change in potential. Figure 2c shows the time-averaged potential distribution within the device when both AC and DC voltages are applied. In this scenario, the voltage drop across the length of the sample channel continues to be strongly influenced by the DC voltage. These results show that a DC voltage can be applied across 'contactless' fluid electrode channels and induce a strong electric field within a sample channel. This field can be used to set up an electroosmotic flow without direct contact between the sample and the electrodes. The application of an AC voltage perpendicular to this DC field appears to have little impact on the potential distribution along the length of the channel, but may potentially affect the EK flow.

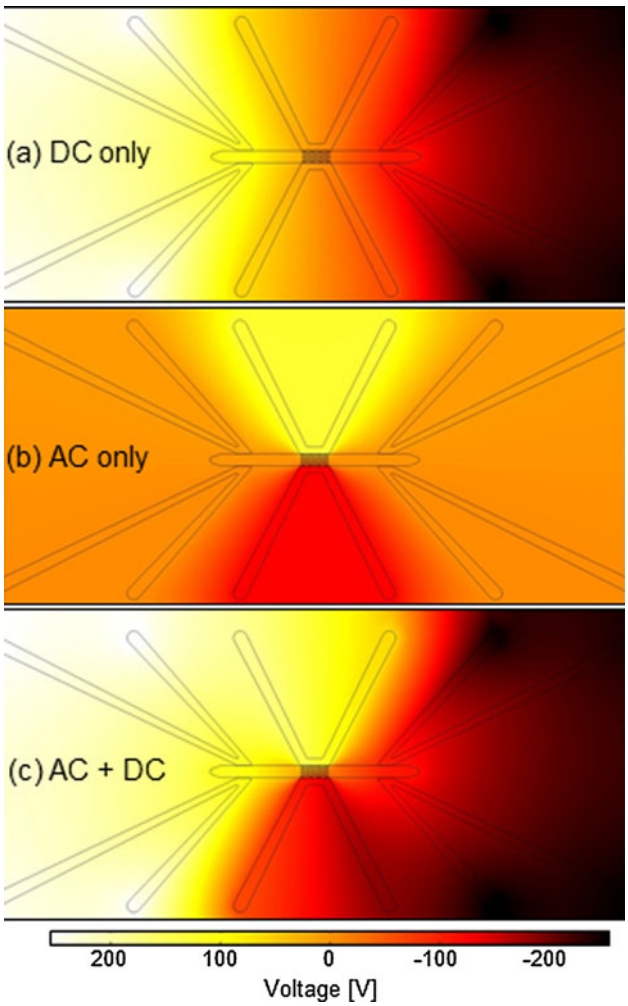


**Fig. 2** Simulation results obtained with COMSOL Multiphysics for the voltage distribution in the device under the following conditions: **a** only the DC fluid electrodes are energized with a total potential of 500 V (±250 $V_{DC}$), **b** only the AC fluid electrodes are energized (250 $V_{RMS}$ at 500 kHz), and **c** when the AC and DC fluid electrodes are simultaneously energized with the same potentials used in (**a**) and (**b**)

The distribution of the potential drop across the sample channel is depicted in Fig. 3a. The total voltage drop across the sample channel from inlet (a) to outlet (a′) is 224.5 V. From the inlet (a) to the exterior edge of the positive DC fluid electrode (b), the potential drop is 6.4 V. From the exterior edge of the positive DC fluid electrode (b) to the interior edge (c), the potential drop is 11.3 V. Between the two DC fluid electrodes, from c to c′, the voltage drop is 190.5 V. The resulting voltage to distance ratio in this segment of the sample channel is 198.7 V/cm. This potential drop produces the electric field which drives the

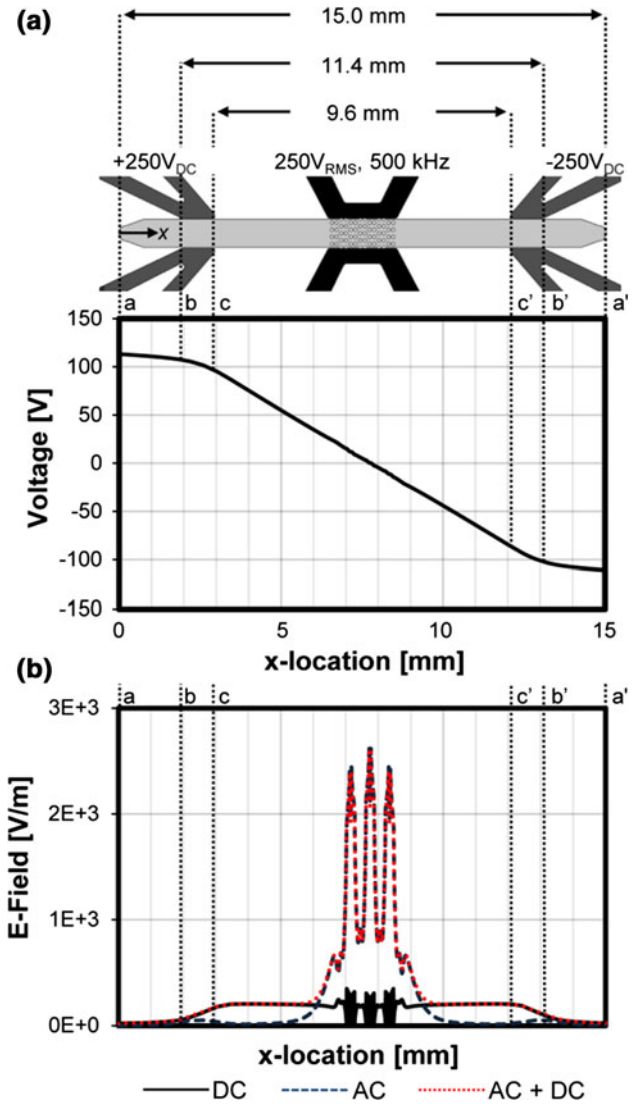


**Fig. 3** **a** Voltage distribution within the sample channel from inlet to outlet when a 500 V ($\pm$250 $V_{DC}$) static potential is applied across the microchannel employing the DC fluid electrodes. A linear regression of this *curve* shows a voltage drop of 198.7 V between *c* and *c*′ **b** electric field distribution generated along the length of the device when 250 $V_{RMS}$ at 500 kHz AC only (*dashed line*) is applied, 500 V DC only (*solid line*), and AC + DC electric fields (*dotted line*) are applied

EK flow. When the system is considered in more fundamental terms as an electrical circuit, the barriers which separate the fluid electrodes from the sample channel and the bulk material which separates all fluid components represent a much larger resistance than any fluid components (as individuals or combined). The fluid channels behave as very small resistances in series with the much larger resistance of the PDMS components. Due to this, a majority of the voltage drop (and resistive losses) occur across the PDMS components

Figure 3b shows the distribution of the electric field across the length of the main channel, when applying only

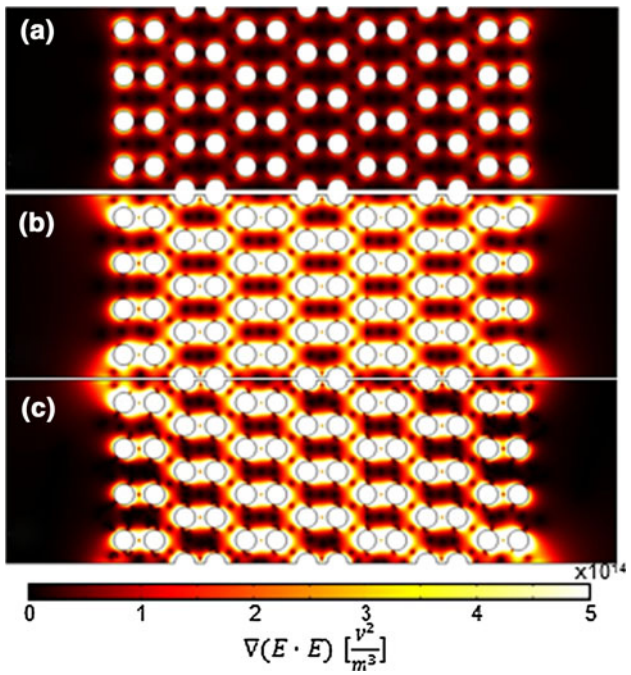


**Fig. 4** DEP field, $\nabla(E{\cdot}E)$, within the sample channel when (**a**) only the DC fluid electrodes are energized with a total potential of 500 V ($\pm$250 $V_{DC}$), **b** only the AC fluid electrodes are energized (250 $V_{RMS}$ at 500 kHz), and **c** when the AC and DC fluid electrodes are simultaneously energized with the same potentials used in (**a**) and (**b**)

a DC potential of 500 V, only an AC potential of 250 $V_{RMS}$ at 500 kHz, and both AC and DC potentials. From Fig. 3b it is observed that the electric field varies significantly only when the AC potential is applied and only across the insulating post region.

Since DEP effects depends directly on the DEP field ($\nabla(E{\cdot}E)$), a set of simulation aimed to study this parameter was carried out. Figure 4a shows the gradient of the electric field squared (DEP field, $\nabla(E{\cdot}E)$) when only the DC voltage is applied. A large DEP field is present close to the top and bottom of each of the pillars. These regions are co-located with regions of high fluid velocity (shown in Fig. 5). Figure 4b shows the DEP field for the scenario when only an AC voltage is applied. The volume of the device in which strong DEP forces occur is substantially larger than in the case of only DC voltage. In addition, the magnitude of the DEP field is elevated in regions between the pairs of posts. In these zones, the fluid velocity is anticipated to be low, improving the probability that particles will become trapped. When the AC and DC fluid electrodes are energized the resulting DEP field, shown in Fig. 4c, becomes slightly distorted. This is due to the interaction of the AC and DC fields and the magnitude of the distortion is anticipated to change with the phase of the AC signal.

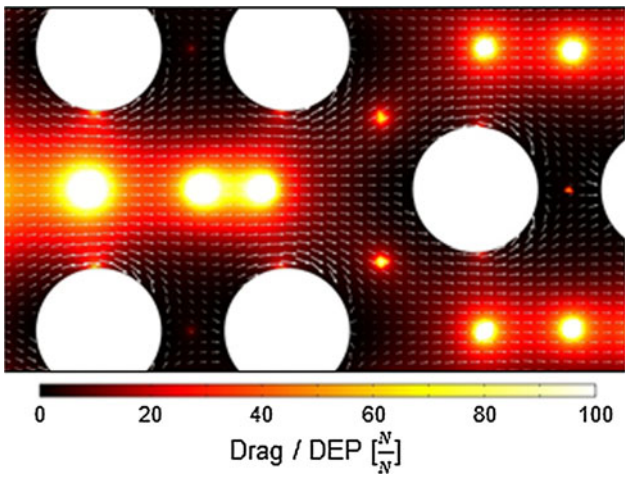


**Fig. 5** Surface plot of the ratio of Drag/DEP forces calculated using experimental parameters (±250 $V_{DC}$ and 250 $V_{RMS}$ at 500 kHz). *Arrow* plots show normalized simulated particle trajectories. Particle trapping is predicted to occur in the *dark regions* where the *arrows* turn and oppose the bulk flow

The surface plot in Fig. 5 shows the ratio of drag to DEP forces when 500 $V_{DC}$ and 250 $V_{RMS}$ are applied. The arrow plots show calculated particle velocities. As anticipated, particle velocities are the greatest in regions where the pillars constrict the channel width. In contrast, there exist regions of relatively low fluid velocity between horizontal pillar pairs. This combined with the high DEP field ($\nabla(E{\cdot}E)$) (Fig. 4c) creates a region of low particle velocity in which the probability of particle trapping is maximized.

### 4.2 Experimental results

When a static voltage was applied across the DC fluid electrodes, electrokinetic flow was induced as shown in Fig. 6a (500 $V_{DC}$). As anticipated, since EK flow has a linear dependence with the electric field (Eq. 1), the velocity of the particles increased as the applied voltage was elevated. Between 50 and 350 $V_{DC}$ the influence of DEP was negligible and the particles mainly moved due to EK flow, only a small number of stray particles adhered to some of the posts and microchannel walls. At 350 $V_{DC}$ and above a small counter current developed along the top edge of the sample channel. A population of particles was observed moving in the opposite direction of the bulk flow. The cause of this counter flow is currently unknown, but it may be a result of the development of pressure or thermal gradients. At these elevated voltages, a small number of particles began to trap at the top and bottom edges of the pillars, as shown in Fig. 6a. The device presented here was specifically designed to minimize the effect of the DC DEP force by increasing the edge-to-edge distance between the pillars in the y-direction.

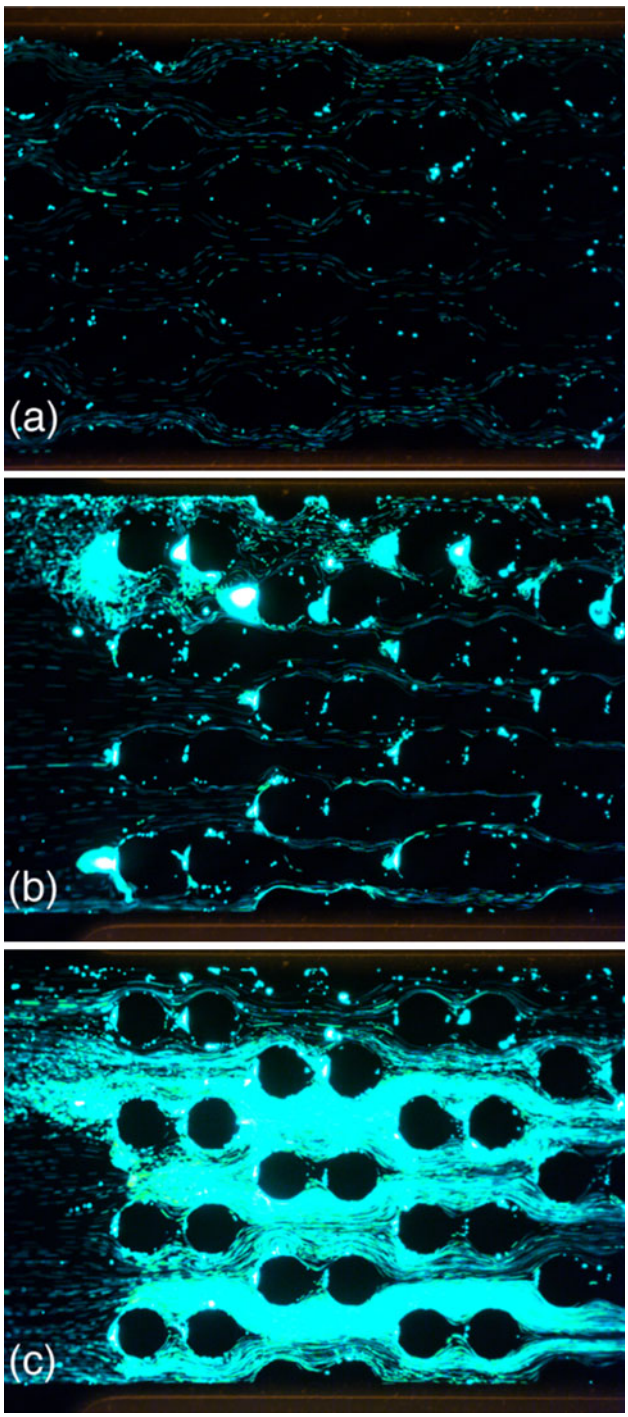


**Fig. 6** Experimental application of electric potentials to the device. **a** When only the DC fluid electrodes are energized to ±250 $V_{DC}$, EK pumping drives the particles from *left* to *right*. **b** When the AC fluid electrodes are simultaneously energized to 250 $V_{RMS}$, particles between to trap around the insulating pillars. **c** After 1 min, the AC potential is turned off and particles are released downstream

As shown in Fig. 6b, when a static voltage of 500 V was applied across the DC fluid electrodes and a 250 $V_{RMS}$ signal was applied across the AC fluid electrodes, particles

began to collect near the pillars due to dielectrophoretic trapping, showing that DEP overcame EK in those regions. In agreement with the theoretical predictions (Fig. 5), most particles collected close to the left and right tangents of the pillars. However, some populations collected in vortices which formed in front of the pillars. The cause of these vortices is currently under investigation and is likely due to the interaction of the AC and DC fields as the AC phase changes. After 1 min, the AC field was turned off while the DC potential was still on and the particles were released downstream (Fig. 6c). Image analysis showed a 9.32-fold increase in per unit area intensity. Trapping efficiency can be increased by lowering the magnitude of the DC potential; however, this results in lower flow rates and total throughput. Alternatively, the center-to-center distance between the pillars in the x-direction can be reduced to increase the total DEP force between the pillars.

Figure 5 shows that in the regions above and below the pillars, fluid drag forces dominate the DEP forces by a factor of 100 or more, predicting high particle trajectories, and minimal trapping in these regions. This correlates well to the experimental results in Fig. 6b, where particles are observed to move at a high velocity in regions where the vertical spacing between pillars is large and the DEP forces due to both the AC and DC fields are small (as shown in Fig. 4). The simulation results in Fig. 5 predict regions of low particle velocity immediately adjacent to the left and right edges of the insulating pillars. A majority of particle trapping was observed to occur at the leading edge of the pillars; however, some particles were trapped in the regions where the horizontal spacing between pillars was small as predicted. Experimentally, vortices formed at the leading edge, and between the pillars, however, the simulations were unable to fully capture this phenomena. Overall, the simulations were able to predict the general behavior of particles within the device under DC, AC, and combined AC/DC fields. However, the accuracy and precision of these models in predicting exact particle velocities has not been evaluated.

## 5 Concluding remarks

The device presented here is the first example of electro-osmotic pumping using physically isolated fluid electrodes. Electrokinetic flow is not necessarily predicated on the flow of current through the insulating barriers, all that is required is the establishment of an electric field (voltage gradient) along the sample channel. In this case, a majority of the voltage drop is due to the resistance of the PDMS which separates the positive and negative DC fluid electrodes. The sample channel has a relatively small resistance compared to the barriers and compared to the resistance of the PDMS device as a whole. In this device configuration, the DC potential of any segment of the sample channel is elevated to the same potential as the PDMS directly adjacent to it, resulting in the necessary voltage drop for establishing EK flow. This technique is advantageous as it eliminates sample-electrode contact and the need for platinum or silver–silver chloride electrodes. Another attractive feature of the combination of cDEP with EO flow is the potential for highly controlled particle manipulation with DEP at much lower applied potentials than traditional iDEP, and with simpler systems that does not require the use of an external pump. This mode of static electric field generation has applications in a number of microfluidic microdevices including cell sorting, trapping, and migration studies. This technique eliminates the need for an external pump in cDEP designs, increasing the portability of the systems. Future work will focus on examination of the vortex phenomena observed during experimentation and investigating the viability of this technique for cell sorting.

**Acknowledgments** This work was funded in part by the Multiscale Bio-Engineered Devices and Systems (MBEDS) group and the Institute for Critical Technology and Applied Science (ICTAS) at Virginia Tech. Additional funding was provided by CONACYT and *Cátedra de Investigación* CAT142 of *Tecnológico de Monterrey*. The authors would like to thank the members of the VT BEMS laboratory, especially Alireza Salmanzadeh, for their help fabricating the silicon master stamps.

**Conflict of interest** Sano and Davalos have a pending patent for contactless dielectrophoresis.

## References

Bao N, Wang J, Lu C (2008) Recent advances in electric analysis of cells in microfluidic systems. Anal Bioanal Chem 391:933–942

Barz DPJ, Ehrhard P (2005) Model and verification of electrokinetic flow and transport in a micro-electrophoresis device. Lab Chip 5:949–958

Baylon-Cardiel JL, Lapizco-Encinas BH, Reyes-Betanzo C, Chávez-Santoscoy AV, Martínez Chapa SO (2009) Prediction of trapping zones in an insulator-based dielectrophoretic device. Lab Chip 9:2896–2901

Baylon-Cardiel JL, Jesús-Pérez NM, Chávez-Santoscoy AV, Lapizco-Encinas BH (2010) Controlled microparticle manipulation employing low frequency alternating electric fields in an array of insulators. Lab Chip 10:3235–3242

Bhattacharya S, Chao T-C, Ros A (2011) Insulator-based dielectrophoretic single particle and single cancer cell trapping. Electrophoresis 32:2550–2558

Chávez-Santoscoy AV, Baylon-Cardiel JL, Moncada-Hernández H, Lapizco-Encinas BH (2011) On the selectivity of an insulator-based dielectrophoretic microdevice. Sep Sci Technol 46:384–394

Cummings EB, Singh AK (2003) Dielectrophoresis in microchips containing arrays of insulating posts: theoretical and experimental results. Anal Chem 75:4724–4731

Docoslis A, Kalogerakis N, Behie LA, Kaler K (1997) A novel dielectrophoresis-based device for the selective retention of viable cells in cell culture media. Biotechnol Bioeng 54:239–250

Ermolina I, Milner J, Morgan H (2006) Dielectrophoretic investigation of plant virus particles: cow pea mosaic virus and tobacco mosaic virus. Electrophoresis 27:3939–3948

Felten M, Geggier P, Jäger M, Duschl C (2006) Controlling electrohydrodynamic pumping in microchannels through defined temperature fields. Phys Fluids 18:051707

Feng J-F, Liu J, Zhang X-Z, Zhang L, Jiang J-Y, Nolta J, Zhao M (2012) Guided migration of neural stem cells derived from human embryonic stem cells by an electric field. Stem Cells 30: 349–355

Gagnon ZR (2011) Cellular dielectrophoresis: applications to the characterization, manipulation, separation and patterning of cells. Electrophoresis 32:2466–2487

Gallo-Villanueva RC, Rodriguez-Lopez CE, Diaz-De-La-Garza RI, Reyes-Betanzo C, Lapizco-Encinas BH (2009) DNA manipulation by means of insulator-based dielectrophoresis employing direct current electric fields. Electrophoresis 30:4195–4205

Gallo-Villanueva RC, Jesús-Pérez NM, Martínez-López JI, Pacheco A, Lapizco-Encinas BH (2011a) Assessment of microalgae viability employing insulator-based dielectrophoresis. Microfluid Nanofluid 10:1305–1315

Gallo-Villanueva RC, Pérez-González VH, Davalos RV, Lapizco-Encinas BH (2011b) Separation of mixtures of particles in a multipart microdevice employing insulator-based dielectrophoresis. Electrophoresis 32:2456–2465

Gencoglu A, Camacho-Alanis F, Nguyen VT, Nakano A, Ros A, Minerick AR (2011) Quantification of pH gradients and implications in insulator-based dielectrophoresis of biomolecules. Electrophoresis 32:2436–2447

Hawkins BG, Kirby BJ (2010) Electrothermal flow effects in insulating (electrodeless) dielectrophoresis systems. Electrophoresis 31:3622–3633

Henslee EA, Sano MB, Rojas AD, Schmelz EM, Davalos RV (2011) Selective concentration of human cancer cells using contactless dielectrophoresis. Electrophoresis 32:2523–2529

Homsy A, Linder V, Lucklum F, de Rooij NF (2007) Magnetohydrodynamic pumping in nuclear magnetic resonance environments. Sens Actuators B Chem 123:636–646

Hughes MP, Hoettges KF (2008) Bacterial concentration, separation and analysis by dielectrophoresis. In: Zourob M, Elwary S, Turner A (eds) Principles of bacterial detection: biosensors, recognition receptors and microsystems. Springer, New York, pp 895–907

Iverson BD, Garimella SV (2008) Recent advances in microscale pumping technologies: a review and evaluation. Microfluid Nanofluid 5:145–174

Ivory CF, Srivastava SK (2011) Direct current dielectrophoretic simulation of proteins using an array of circular insulating posts. Electrophoresis 32:2323–2330

Jaramillo MdC, Torrents E, Martínez-Duarte R, Madou MJ, Juárez A (2010) On-line separation of bacterial cells by carbon-electrode dielectrophoresis. Electrophoresis 31:2921–2928

Jones P, Staton S, Hayes M (2011) Blood cell capture in a sawtooth dielectrophoretic microchannel. Anal Bioanal Chem 401:2103–2111

Kang YJ, Li DQ (2009) Electrokinetic motion of particles and cells in microchannels. Microfluid Nanofluid 6:431–460

Kwon J-S, Maeng J-S, Chun M-S, Song S (2008) Improvement of microchannel geometry subject to electrokinesis and dielectrophoresis using numerical simulations. Microfluid Nanofluid 5:23–31

Lapizco-Encinas BH, Ozuna-Chacón S, Rito-Palomares M (2008) Protein manipulation with insulator-based dielectrophoresis and DC electric fields. J Chromatogr A 1206:45–51

Leonard KM, Minerick AR (2011) Explorations of ABO-Rh antigen expressions on erythrocyte dielectrophoresis: changes in cross-over frequency. Electrophoresis 32:2512–2522

Lin Q, Yang BZ, Xie J, Tai YC (2007) Dynamic simulation of a peristaltic micropump considering coupled fluid flow and structural motion. J Micromech Microeng 17:220–228

Machauf A, Nemirovsky Y, Dinnar U (2005) A membrane micropump electrostatically actuated across the working fluid. J Micromech Microeng 15:2309–2316

Martinez-Duarte R, Gorkin-Iii RA, Abi-Samra K, Madou MJ (2010) The integration of 3D carbon-electrode dielectrophoresis on a CD-like centrifugal microfluidic platform. Lab Chip 10:1030–1043

Martinez-Duarte R, Renaud P, Madou MJ (2011) A novel approach to dielectrophoresis using carbon electrodes. Electrophoresis 32: 2385–2392

Matteucci M, Perennes F, Marmiroli B, Miotti P, Vaccari L, Gosparini A, Turchet A, Di Fabrizio E (2006) Compact micropumping system based on LIGA fabricated microparts. Microelectron Eng 83:1288–1290

Moncada-Hernández H, Lapizco-Encinas BH (2010) Simultaneous concentration and separation of microorganisms: insulator-based dielectrophoretic approach. Anal Bioanal Chem 396(5):1805–1816

Moncada-Hernández H, Baylon-Cardiel JL, Pérez-González VH, Lapizco-Encinas BH (2011) Insulator-based dielectrophoresis of microorganisms: theoretical and experimental results. Electrophoresis 32:2502–2511

Pohl HA (1958) Some effects of nonuniform fields on dielectrics. J Appl Phys 29:1182–1188

Pysher MD, Hayes MA (2007) Electrophoretic and dielectrophoretic field gradient technique for separating bioparticles. Anal Chem 79:4552–4557

Regtmeier J, Eichhorn R, Bogunovic L, Ros A, Anselmetti D (2010) Dielectrophoretic trapping and polarizability of DNA: the role of spatial conformation. Anal Chem 82:7141–7149

Sano MB, Caldwell JL, Davalos RV (2011a) Modeling and development of a low frequency contactless dielectrophoresis (cDEP) platform to sort cancer cells from dilute whole blood samples. Biosens Bioelectron 30:13–20

Sano MB, Henslee EA, Schmelz E, Davalos RV (2011b) Contactless dielectrophoretic spectroscopy: examination of the dielectric properties of cells found in blood. Electrophoresis 32:3164–3171

Shafiee H, Caldwell JL, Sano MB, Davalos RV (2009) Contactless dielectrophoresis: a new technique for cell manipulation. Biomed Microdevices 11:997–1006

Shafiee H, Caldwell JL, Davalos RV (2010a) A microfluidic system for biological particle enrichment using contactless dielectrophoresis. Jala 15:224–232

Shafiee H, Sano MB, Henslee EA, Caldwell JL, Davalos RV (2010b) Selective isolation of live/dead cells using contactless dielectrophoresis (cDEP). Lab Chip 10:438–445

Sridharan S, Zhu J, Hu G, Xuan X (2011) Joule heating effects on electroosmotic flow in insulator-based dielectrophoresis. Electrophoresis 32:2274–2281

Srivastava SK, Artemiou A, Minerick AR (2011a) Direct current insulator-based dielectrophoretic characterization of erythrocytes: ABO-Rh human blood typing. Electrophoresis 32:2530–2540

Srivastava SK, Gencoglu A, Minerick AR (2011b) DC insulator dielectrophoretic applications in microdevice technology: a review. Anal Bioanal Chem 399:301–321

Sun Y-S, Peng S-W, Lin K-H, Cheng J-Y (2012) Electrotaxis of lung cancer cells in ordered three-dimensional scaffolds. Biomicrofluidics 6:014102–014114

Tandon V, Bhagavatula SK, Nelson WC, Kirby BJ (2008) Zeta potential and electroosmotic mobility in microfluidic devices fabricated from hydrophobic polymers: 1. The origins of charge. Electrophoresis 29:1092–1101

Ugaz VM, Christensen JL (2007) Electrophoresis in microfluidic system. In: Hardt S, Schonfeld F (eds) Microfluidic technologies for miniaturized analysis systems. Springer, New York, pp 393–438

Voldman J (2006) Electrical forces for microscale cell manipulation. Annu Rev Biomed Eng 8:425–454

Voyer D, Frenea-Robin M, Buret F, Nicolas L (2010) Improvements in the extraction of cell electric properties from their electrorotation spectrum. Bioelectrochemistry 79:25–30

Whitesides GM (2006) The origins and the future of microfluidics. Nature 442:368–373

Yang L, Bashir R (2008) Electrical/electrochemical impedance for rapid detection of foodborne pathogenic bacteria. Biotechnol Adv 26:135–150

Yang F, Yang X, Jiang H, Bulkhaults P, Wood P, Hrushesky W, Wang G (2010) Dielectrophoretic separation of colorectal cancer cells. Biomicrofluidics 4:013204–013213